Thermal Behavior of Hydrated Iron Sulfate in Various Atmospheres

Ndue Kanari, Nour-Eddine Menad, Etleva Ostrosi, Seit Shallari, Frédéric Diot, Eric Allain, Jacques Yvon

metals

MDPI

Article

Thermal Behavior of Hydrated Iron Sulfate in Various Atmospheres

Ndue Kanari [1,*], Nour-Eddine Menad [2], Etleva Ostrosi [3], Seit Shallari [4], Frederic Diot [1], Eric Allain [1] and Jacques Yvon [1]

1 GeoRessources Laboratory, UMR 7359 CNRS, CREGU, Université de Lorraine, 2, rue du doyen Roubault, BP 10162, 54505 Vandoeuvre-lès-Nancy, France; frederic.diot@univ-lorraine.fr (F.D.); ericgallain@gmail.com (E.A.); jacques.yvon@univ-lorraine.fr (J.Y.)
2 BRGM, 3 av. C. Guillemin, BP 36009, CEDEX 2, 45060 Orléans, France; N.Menad@brgm.fr
3 Ville de Montréal, Direction de l'Environnement, Division de la Planification et du Suivi Environnemental, 801, rue Brennan, Montréal, QC H3C 0G4, Canada; etlevao@yahoo.com
4 Faculty of Agriculture and Environment, Agriculture University of Tirana, 1029 Tirana, Albania; seitshallari@gmail.com
* Correspondence: ndue.kanari@univ-lorraine.fr; Tel.: +33-372-744-530

Received: 19 November 2018; Accepted: 13 December 2018; Published: 19 December 2018

Abstract: Iron sulfate, in particular $FeSO_4 \cdot 7H_2O$, is derived from titanium dioxide production and the steel pickling process. Regarding TiO_2 manufacturing, the amount of the resultant $FeSO_4 \cdot 7H_2O$ can be as high as 6 tons per ton of produced TiO_2, leading to a huge amount of ferrous sulfate heptahydrate, which is considered an environmental and economic concern for the titanium dioxide industry in European countries. The present paper focuses on the thermal treatment of ferrous sulfate (heptahydrate and monohydrate) samples under different conditions. Nonisothermal thermogravimetric (TG) analysis was used to study the behavior of iron sulfate samples at temperatures of up to 1000 °C in $Cl_2 + O_2$, O_2, and N_2 atmospheres. Results showed that the dehydration of iron sulfate heptahydrate in nitrogen started at room temperature and resulted in iron sulfate tetrahydrate ($FeSO_4 \cdot 4H_2O$). The ferrous sulfate monohydrate ($FeSO_4 \cdot H_2O$) was formed at temperatures close to 150 °C, while the anhydrous ferrous sulfate ($FeSO_4$) was obtained when the samples were heated in nitrogen at over 225 °C. The kinetic features of $FeSO_4$ decomposition into Fe_2O_3 were revealed under isothermal conditions at temperatures ranging from 500 to 575 °C. The decomposition of iron sulfate was characterized by an apparent activation energy of around 250 kJ/mol, indicating a significant temperature effect on the decomposition process. The obtained powder iron oxide could be directed to the agglomeration unit of iron and the steelmaking process.

Keywords: iron sulfate; TG analysis; thermal treatment; iron oxide; kinetics; activation energy

1. Introduction

Titanium oxide (TiO_2) is manufactured from materials such as ilmenite, rutile, anatase, and slags using sulfate or chloride processes. The simplified schemes for the industrial processes that are currently used are presented in Figure 1 [1]. Ilmenite and titanium slags are the raw materials used for TiO_2 manufacturing through the sulfate process. The ilmenite is digested in sulfuric acid, generating a solution that contains titanyl sulfate ($TiOSO_4$) and iron sulfate. The solution is treated with scrap iron to reduce the ferric ions into a ferrous state to avoid the precipitation of ferric hydroxide. The ferrous sulfate then crystallizes into $FeSO_4 \cdot 7H_2O$ (melanterite) and is separated from the liquor. Additional steps (see Figure 1) are necessary to obtain the TiO_2 base pigment. Depending on the quality of the raw materials used in the TiO_2 production, the amount of iron sulfate produced can reach up to 6 tons

of $FeSO_4 \cdot 7H_2O$ per ton of produced TiO_2 when ilmenite is used as the raw material. The sulfate route, which is mainly used in the production of TiO_2 in European countries, generates a huge amount of wasted ferrous sulfate heptahydrate. On the contrary, North American countries produce TiO_2 through the chlorine route, the main steps of which are also shown in Figure 1.

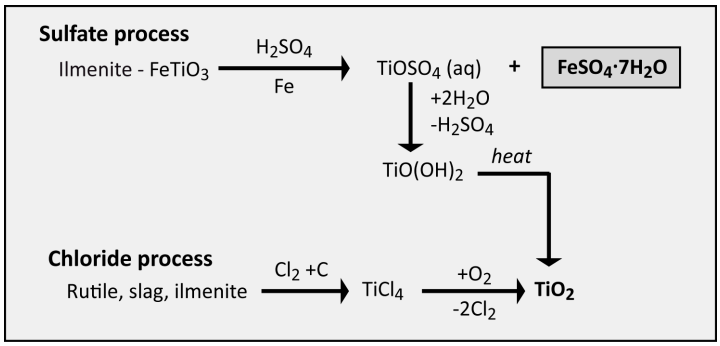

Figure 1. Schematic representation of the main steps in titanium oxide manufacturing using sulfate and chloride processes, adapted from Reference [1].

An extensive overview of the titanium metallurgical processes was recently conducted in Reference [2]. This report compares the main characteristics of the classical and emerging processes for TiO_2 manufacturing from economic and environmental viewpoints. As mentioned in earlier works [3,4], one drawback of the sulfate process is the amount of iron sulfate heptahydrate and the spent acid generated during TiO_2 production. Only a small part of the iron sulfate is reused, and the remaining part must be disposed of as waste. It must be noted that the amount of $FeSO_4 \cdot 7H_2O$ generated from the surface treatment of steel is decreasing due to the use of hydrochloric acid (HCl) instead of sulfuric acid (H_2SO_4).

Several investigations previously conducted in our laboratory were focused on the use of industrial iron sulfate for the synthesis of alkali ferrates [3,5,6]. The potassium ferrate synthesis (K_2FeO_4) from spent steel pickling liquid was also reported by Wei et al. [7]. A recent work applied the reductive decomposition reaction of iron sulfate with pyrite into Fe_3O_4 at a relatively low temperature [4].

In this context, the present work dealt with the dehydration and the decomposition of various iron sulfate samples in oxidizing and neutral atmospheres. Thermogravimetric (TG) analysis was used as an appropriate method to continuously follow the reaction kinetics in the decomposition of $FeSO_4$ into iron oxide under isothermal conditions. The iron oxide obtained can be used as a raw material in the ironmaking sectors. Many recent reports are available on the reduction of iron-oxide-bearing materials from various known agents [8–16].

2. Materials and Methods

Several samples of the iron sulfate heptahydrate generated from industrial operators were collected, the physicochemical characterization of which has been previously given in Reference [3]. For this investigation, two samples of iron sulfate were selected. The first sample—iron sulfate monohydrate—was provided by an industrial operator and was named the IND sample. The second sample—LAB sample—was obtained through the two-step dehydration process of analytical-grade iron sulfate heptahydrate ($FeSO_4 \cdot 7H_2O$) in a laboratory oven. The heating of the $FeSO_4 \cdot 7H_2O$ at about 60–70 °C led to the loss of 3 mol of water, resulting in the formation of $FeSO_4 \cdot 4H_2O$. An increase in the temperature to about 150 °C provoked the dehydration of the iron sulfate tetrahydrate into $FeSO_4 \cdot H_2O$. However, in the presence of air, the oxidation of Fe(II) into Fe(III) may occur. Both the IND and LAB samples were subjected to a variety of analyses to determine their composition.

The total iron and Fe(II) contents of the samples were determined using chemical analysis. After sample digestion, the Fe(II) was determined using potassium dichromate titration. Table 1 gives

the average values of iron in both the samples. The IND sample contained about 31% Fe, and the whole iron was in a divalent state. X-Ray diffraction (XRD) analysis only showed the presence of $Fe^{II}SO_4 \cdot H_2O$ in the crystallized phase. The total iron content of the LAB sample was 32.8% in which 14.8% was in a divalent state and 18.0% was in a trivalent state. In other words, in the 100% Fe_{total} LAB sample, about 45% was Fe(II) and about 55% was Fe(III). Concerning the results of XRD (see Table 1), they revealed the presence of $Fe^{II}SO_4 \cdot H_2O$ and $Fe^{III}SO_4 \cdot OH$ in the LAB sample. This confirmed that the dehydration of $FeSO_4 \cdot 4H_2O$ into $FeSO_4 \cdot H_2O$ and partial oxidation of Fe(II) to Fe(III) occurred by 150 °C.

Table 1. Results of chemical and XRD analysis of two iron sulfate samples.

Sample	Chemical Analysis (%)			XRD
	Fe_{total}	Fe(II)	Fe(III)	
IND	30.9	30.9	trace	$Fe^{II}SO_4 \cdot H_2O$
LAB	32.8	14.8	18.0 [1]	$Fe^{II}SO_4 \cdot H_2O$ and $Fe^{III}SO_4 \cdot OH$

[1] By difference.

Experimental tests of thermogravimetric analysis were performed using a CAHN 1000 microbalance capable of resisting corrosive atmospheres to check the thermal behavior of $FeSO_4 \cdot 7H_2O$ under different atmospheres (Cl_2 + O_2, Cl_2, O_2, and N_2). Furthermore, a TG 2171 Cahn balance was used to study the dehydration/decomposition kinetics of iron sulfate samples under N_2 by simultaneous TG and differential thermal (DT) measurements. Solid reaction products were examined by X-ray diffraction, scanning electron microscopy, and Mössbauer spectroscopy.

3. Results

3.1. Nonisothermal TG Analysis of $FeSO_4 \cdot 7H_2O$ under Different Atmospheres

The thermal behavior of a $FeSO_4 \cdot 4H_2O$ sample in various gaseous atmospheres (Cl_2 + O_2, O_2, and N_2) was investigated by TG analysis utilizing nonisothermal conditions [3]. The results are drawn in Figure 2 as the evolution of the percent mass loss (% ML) of the sample versus temperature up to 300 °C. The calculated limits corresponding to different hydrated states of ferrous sulfate are also shown in Figure 2. Results of XRD and Mössbauer analyses [1] showed that $FeSO_4 \cdot 4H_2O$, $FeSO_4 \cdot H_2O$, and $FeSO_4$ are the main crystallized phases in the solid product obtained at 75 °C, 150 °C and 300 °C, respectively, during the treatment of iron sulfate heptahydrate sample under nitrogen atmosphere. Conversely, the treatment of the sample under oxidizing atmosphere (Cl_2 + O_2, O_2) led to the transformation of Fe(II) into Fe(III), and the product obtained at 300 °C was mainly composed of $FeSO_4 \cdot OH$.

As revealed by Mössbauer analysis, the product resulting from the treatment of $FeSO_4 \cdot 7H_2O$ in N_2 at 150 °C was composed of Fe(II) in totality, while the product generated by the treatment in Cl_2 + O_2 contained iron, mostly in a three-valent state. To observe the reactivity of iron sulfate toward O_2 and Cl_2 + O_2, TG tests were performed at temperatures up to 1000 °C, and the corresponding data is plotted in Figure 3. As can be seen, the curves for both oxidizing gas mixtures have roughly similar shapes for temperatures up to 675 °C. This observation suggests that chlorine reacted with the sample only after the decomposition of iron sulfate into ferric oxide (hematite), producing ferric chloride ($FeCl_3$) as a final reaction product [3]. The kinetics of the reaction of Fe_2O_3 with Cl_2 and Cl_2 + O_2 were further discussed in earlier articles [17,18].

The treatment of $FeSO_4 \cdot 7H_2O$ in nitrogen at different heating rates was followed by DT analysis, and a data summary is given in Table 2. These results, combined with those of TG analysis and XRD analysis, show that the sequence of sample transformation was the following: $FeSO_4 \cdot 7H_2O \rightarrow FeSO_4 \cdot 4H_2O \rightarrow FeSO_4 \cdot H_2O \rightarrow FeSO_4 \rightarrow Fe_2O_3$.

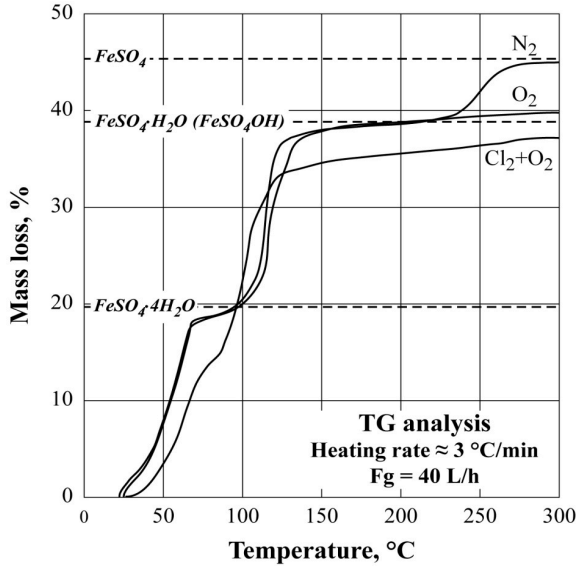

Figure 2. Thermogravimetric (TG) analysis of a $FeSO_4 \cdot 7H_2O$ sample under different atmospheres.

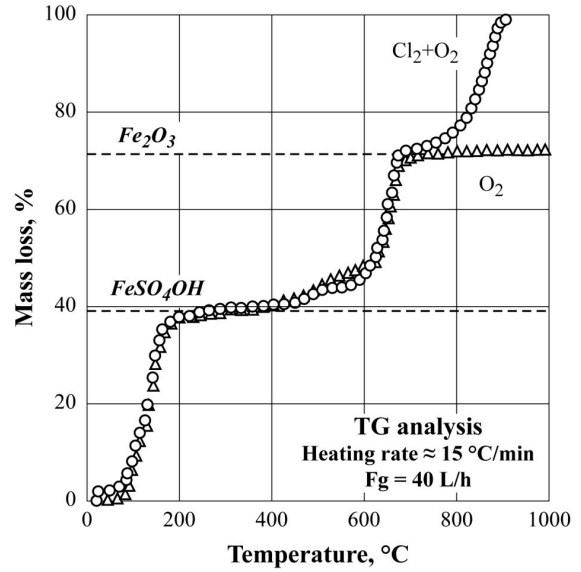

Figure 3. TG analysis of a $FeSO_4 \cdot 7H_2O$ sample in O_2 and Cl_2 + O_2 atmospheres.

Table 2. Endothermic peaks (°C) revealed by differential thermal (DT) analysis for the treatment of $FeSO_4 \cdot 7H_2O$ under nitrogen at various heating rates.

Heating Rate, °C/min			Possible Reaction Steps		
2.5	**5.0**	**10.0**			
70	80	98	$FeSO_4 \cdot 7H_2O$	→	$FeSO_4 \cdot 4H_2O$
86	133	159	$FeSO_4 \cdot 4H_2O$	→	$FeSO_4 \cdot H_2O$
227	250	283	$FeSO_4 \cdot H_2O$	→	$FeSO_4$
653	687	716	$FeSO_4$	→	Fe_2O_3

3.2. Nonisothermal TG Analysis of $FeSO_4 \cdot H_2O$ under Nitrogen

Nonisothermal TG tests up to 1000 °C in nitrogen were performed for both IND and LAB samples. The furnace heating rates were fixed at 2.5 and 20.0 °C/min, and the data is plotted as the evolution of the % ML as a function of temperature. Figure 4 shows the results for the IND sample. The % ML obtained between 200 and 400 °C corresponds to the dehydration of $FeSO_4 \cdot H_2O$

into $FeSO_4$. The theoretical % ML for the dehydration of iron sulfate monohydrate into iron sulfate (dashed horizontal line) matches well with the experimental % ML of this sample. As shown in Figure 5, the behavior of the LAB sample seems to be somewhat different when compared with the IND sample. Only 7% ML was observed at temperatures less than or equal to 400 °C. This could be attributed to the dehydration of $FeSO_4 \cdot H_2O$ into $FeSO_4$. The continuous mass loss of the LAB sample between 400 and 550 °C was probably due to the transformation of $FeSO_4 \cdot OH$ into ferric oxysulfate ($Fe_2O(SO_4)_2$). The decomposition of iron sulfates producing ferric oxides takes place at temperatures higher than 575 °C, and the curve shapes for both samples seem to be similar. The XRD analysis of the decomposition product showed the presence of Fe_2O_3 in the main crystallized phase.

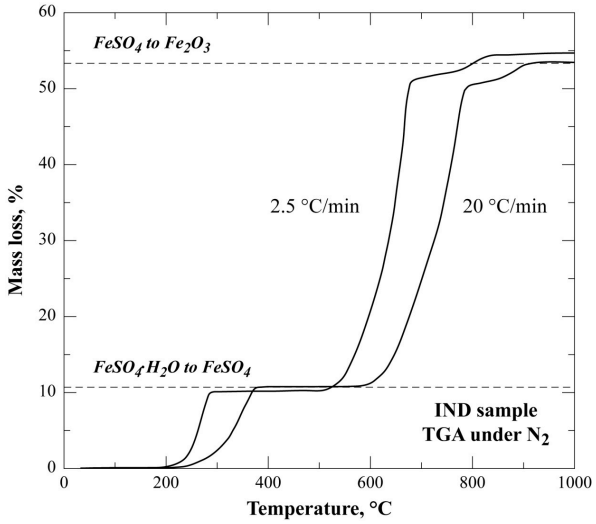

Figure 4. TG analysis in N_2 of the IND sample.

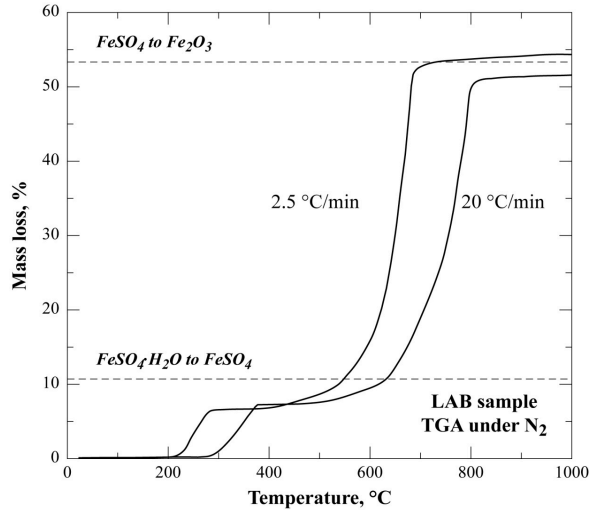

Figure 5. TG analysis in N_2 of the LAB sample.

Based on these TG results, the decomposition kinetics in nitrogen atmosphere of both iron sulfate samples into iron oxide were studied under isothermal conditions at temperatures higher than or equal to 500 °C.

3.3. Isothermal Decomposition of $FeSO_4 \cdot H_2O$ Samples

This decomposition process was tested at low temperatures (between 500 and 575 °C) to minimize the iron sulfate decomposition during the nonisothermal temperature rise. Thus, the initial temperature increased linearly (heating rate = 5.0 °C/min) up to a fixed value, then the temperature remained

constant, and the decomposition extent followed a function of time. A typical example of experimental conditions and results is given in Figure 6. The temperature profile was programmed to increase up to 560 °C; from this point, the decomposition rate (% ML vs. time) was measured at 560 °C. It should be noted that the % ML observed during nonisothermal test (≤12% ML) corresponds to the dehydration step of $FeSO_4 \cdot H_2O$ to $FeSO_4$.

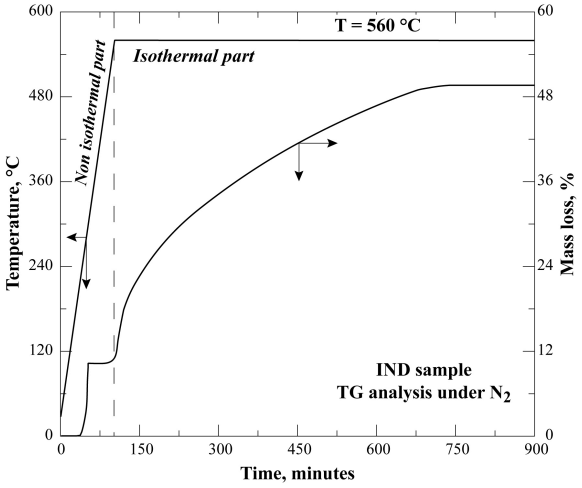

Figure 6. Typical example of TG analysis results of iron sulfate decomposition.

The behavior of both IND and LAB samples under isothermal treatment was monitored in order to check the eventual impact of Fe(III) sulfate on the transformation kinetics. The results obtained from the treatment of the IND sample in nitrogen are represented in Figure 7. About 50 h were necessary for the half decomposition of iron sulfate at 500 °C, while full decomposition was achieved in less than 7 h at 575 °C. This result seems to indicate that the decomposition process depends highly on the temperature.

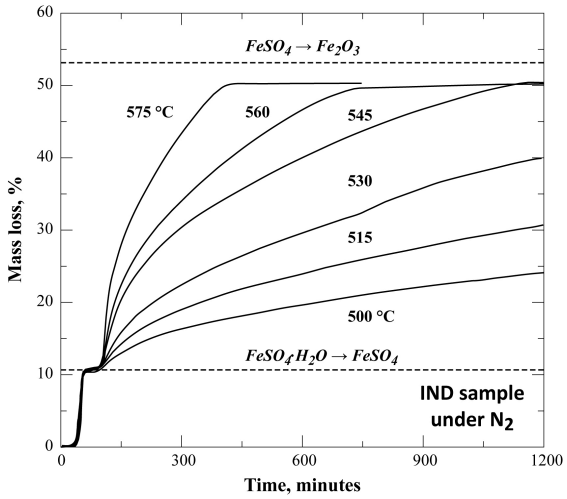

Figure 7. Evolution of the percent mass loss (% ML) as a function of time during the isothermal treatment of an industrial sample under nitrogen between 500 and 575 °C.

Experimental results corresponding to the treatment of LAB sample are illustrated in Figure 8 as % ML versus time for temperatures ranging from 500 to 575 °C. The isothermal part (≥12% ML) of the curves has a similar shape to that observed in the IND sample. When the temperature was increased from 500 to 575 °C, the initial decomposition rate was multiplied by a factor of about 26.

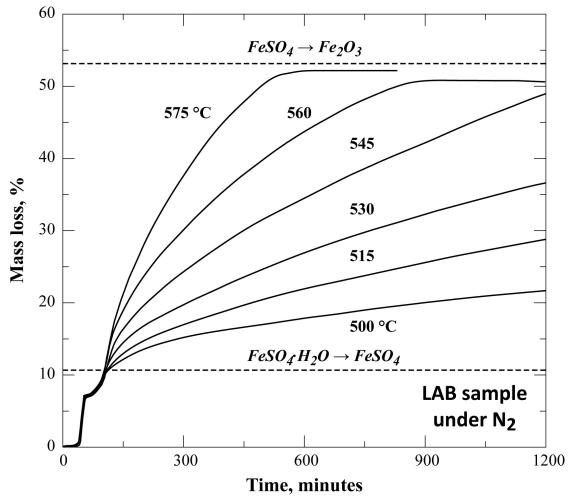

Figure 8. Evolution of the % ML as a function of time during the isothermal treatment of a laboratory sample under nitrogen between 500 and 575 °C.

Arrhenius diagrams for both samples were established in order to evaluate the temperature effect on the initial decomposition rate of iron sulfates. The mean decomposition rate was calculated by linearization of the isothermal data corresponding to 12.5% $\leq$ ML $\leq$ 22.5%. As shown in Figure 9, the decomposition rate of the IND sample was higher than that for the LAB sample over the complete range of temperatures. The values of the apparent activation energy for the treatment of industrial and laboratory sample were about 262 and 238 kJ/mol, respectively, showing the strong effect of temperature on the decomposition process of iron sulfate between 500 and 575 °C. A similar value of apparent activation energy (average value of 244 kJ/mol) was obtained in the work reported by Huang et al. [4].

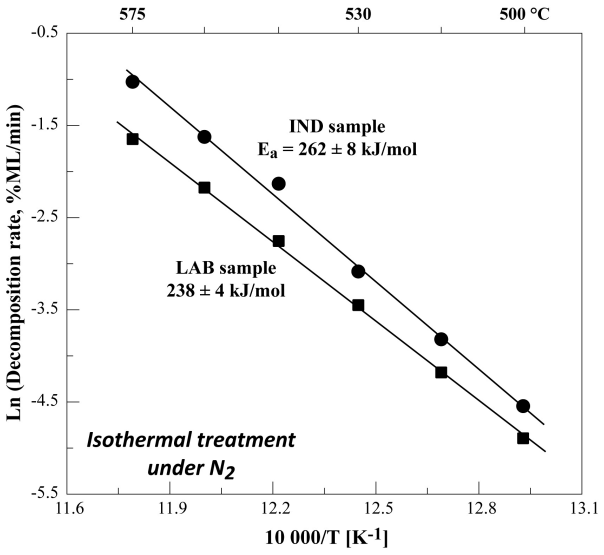

Figure 9. Arrhenius diagram for the decomposition of the iron sulfate samples under nitrogen for temperatures ranging from 500 to 575 °C.

The reaction product generated by the thermal treatment of iron sulfates was mainly composed of pure iron (III) oxide. Such a material, in powder state, must be agglomerated before use for pig iron production and/or for more valuable end uses, such as high-grade pigments for cosmetics.

4. Conclusions

The dehydration of iron sulfate heptahydrate ($FeSO_4 \cdot 7H_2O$) in nitrogen occurred through at least three steps: $FeSO_4 \cdot 7H_2O \rightarrow FeSO_4 \cdot 4H_2O \rightarrow FeSO_4 \cdot H_2O \rightarrow FeSO_4$. Complete dehydration of $FeSO_4 \cdot 7H_2O$ occurred at a temperature lower than 300 °C. The treatment of $FeSO_4 \cdot 7H_2O$ under oxidizing atmosphere led to the formation of $Fe^{III}SO_4 \cdot OH$ as a final stable product at 300 °C.

The decomposition of iron sulfates ($FeSO_4$ and $Fe^{III}SO_4 \cdot OH$) generating ferric oxide, in nonisothermal conditions, started at T > 500 °C, and the final temperature of their full decomposition depended on the heating rate in the furnace.

The isothermal decomposition of selected iron sulfate samples was strongly affected by temperature as it proceeded with a value of apparent activation energy of 250 kJ/mol between 500 and 575 °C. The obtained iron oxide could be used as an appropriate raw material in the ferrous metallurgy sector and/or for more noble end uses.

Author Contributions: Conceptualization, N.K., N.-E.M. and E.O.; Formal analysis, N.-E.M. and E.O.; Investigation, N.K., E.O. and F.D.; Visualization, S.S. and F.D.; Resources, F.D. and J.Y.; Writing—original draft, N.K., E.O., S.S. and E.A.; Writing—review and editing, N.K., E.O, E.A. and J.Y.

Funding: A part of this work was performed in the frame of contract No. BRPR-CT97-0392 of the European Union. Another part of this development work was supported by the French National Research Agency through the program "Investissements d'avenir" with the reference ANR-10-LABX-21-01/LABEX RESSOURCES21.

Conflicts of Interest: The authors declare no conflict of interest.

References

1. Kanari, N. *Contribution to Chlorine Chemistry and its Applications: Synthesis of Alkali Ferrates (VI). A Study of the Kinetics of Chlorine-Solid Reactions*; Defense of the Habilitation Diploma (HDR), Institut National Polytechnique de Lorraine: Nancy, France, 2000.
2. Zhang, W.; Zhu, Z.; Cheng, C.Y. A literature review of titanium metallurgical processes. *Hydrometallurgy* **2011**, *108*, 177–188. [CrossRef]
3. Kanari, N.; Filippova, I.; Diot, F.; Mochón, J.; Ruiz-Bustinza, I.; Allain, E.; Yvon, J. Utilization of a waste from titanium oxide industry for the synthesis of sodium ferrate by gas-solid reactions. *Thermochim. Acta* **2014**, *575*, 219–225. [CrossRef]
4. Huang, P.; Deng, S.; Zhang, Z.; Wang, X.; Chen, X.; Yang, X.; Yang, L. A sustainable process to utilize ferrous sulfate waste from titanium oxide industry by reductive decomposition reaction with pyrite. *Thermochim. Acta* **2015**, *620*, 18–27. [CrossRef]
5. Kanari, N.; Ostrosi, O.; Ninane, N.; Neveux, N.; Evrard, O. Synthesizing alkali ferrates using a waste as a raw material. *JOM* **2005**, *57*, 39–42. [CrossRef]
6. Kanari, N. Method of Producing Ferrates (VI). French Patent n° 2 905 609, 14 March 2008.
7. Wei, Y.-L.; Wang, Y.-S.; Liu, C.-H. Preparation of potassium ferrate from spent steel pickling liquid. *Metals* **2015**, *5*, 1770–1787. [CrossRef]
8. Pineau, A.; Kanari, N.; Gaballah, I. Kinetics of reduction of iron oxides by H_2: Part I: Low temperature reduction of hematite. *Thermochim. Acta* **2006**, *447*, 89–100. [CrossRef]
9. Jozwiak, W.K.; Kaczmarek, E.; Maniecki, T.P.; Ignaczak, W.; Maniukiewicz, W. Reduction behavior of iron oxides in hydrogen and carbon monoxide atmospheres. *Appl. Catal. A* **2007**, *326*, 17–27. [CrossRef]
10. Pineau, A.; Kanari, N.; Gaballah, I. Kinetics of reduction of iron oxides by H_2: Part II. Low temperature reduction of magnetite. *Thermochim. Acta* **2007**, *456*, 75–88. [CrossRef]
11. Tang, J.; Chu, M.S.; Ying, Z.W.; Li, F.; Feng, C.; Liu, Z.G. Non-isothermal gas-based direct reduction behavior of high chromium vanadium-titanium magnetite pellets and the melting separation of metallized pellets. *Metals* **2017**, *7*, 153. [CrossRef]
12. Cao, Y.; Zhang, Y.; Sun, T. Dephosphorization behavior of high-phosphorus oolitic hematite-solid waste containing carbon briquettes during the process of direct reduction-magnetic separation. *Metals* **2018**, *8*, 897. [CrossRef]
13. Oh, J.; Noh, D. The reduction kinetics of hematite particles in H_2 and CO atmospheres. *Fuel* **2017**, *196*, 144–153. [CrossRef]

14. Chen, Z.; Dang, J.; Hu, X.; Yan, H. Reduction kinetics of hematite powder in hydrogen atmosphere at moderate temperatures. *Metals* **2018**, *8*, 751. [CrossRef]
15. Tang, H.; Yun, Z.; Fu, X.; Du, S. Modeling and experimental study of ore-carbon briquette reduction under $CO–CO_2$ atmosphere. *Metals* **2018**, *8*, 205. [CrossRef]
16. Fukushima, J.; Takizawa, H. In situ spectroscopic analysis of the carbothermal reduction process of iron oxides during microwave irradiation. *Metals* **2018**, *8*, 49. [CrossRef]
17. Kanari, N.; Mishra, D.; Filippov, L.; Diot, F.; Mochón, J.; Allain, E. Kinetics of hematite chlorination with Cl_2 and Cl_2+O_2: Part I. Chlorination with Cl_2. *Thermochim. Acta* **2010**, *497*, 52–59. [CrossRef]
18. Kanari, N.; Mishra, D.; Filippov, L.; Diot, F.; Mochón, J.; Allain, E. Kinetics of hematite chlorination with Cl_2 and Cl_2+O_2. Part II. Chlorination with Cl_2+O_2. *Thermochim. Acta* **2010**, *506*, 34–40. [CrossRef]